

RSC Advances



This is an *Accepted Manuscript*, which has been through the Royal Society of Chemistry peer review process and has been accepted for publication.

Accepted Manuscripts are published online shortly after acceptance, before technical editing, formatting and proof reading. Using this free service, authors can make their results available to the community, in citable form, before we publish the edited article. This *Accepted Manuscript* will be replaced by the edited, formatted and paginated article as soon as this is available.

You can find more information about *Accepted Manuscripts* in the [Information for Authors](#).

Please note that technical editing may introduce minor changes to the text and/or graphics, which may alter content. The journal's standard [Terms & Conditions](#) and the [Ethical guidelines](#) still apply. In no event shall the Royal Society of Chemistry be held responsible for any errors or omissions in this *Accepted Manuscript* or any consequences arising from the use of any information it contains.

ARTICLE

Tribological properties of nanodiamonds in aqueous suspensions: effect of the surface charge

Cite this: DOI: 10.1039/x0xx00000x

Zijian Liu,^a Dustin Leininger,^a Amir Koolivand,^a Alex I. Smirnov,^a Olga Shenderova,^b Donald W. Brenner^a and Jacqueline Krim^a

Received 17th July 2015,
Accepted 06th September 2015

DOI: 10.1039/x0xx00000x

www.rsc.org/

Surface uptake and nanotribological properties of positively and negatively charged 5-15 nm diameter nanodiamonds dispersed in water have been studied in real time by means of an *in situ* Quartz Crystal Microbalance (QCM) technique. The frequency and dissipative properties (mechanical resistance) of a QCM with gold surface electrodes immersed in water were monitored upon addition of the nanodiamonds. Measurements were also performed with the QCM electrode in a macroscopic contact with stainless steel ball bearings in the presence or absence of the positively or negatively charged nanodiamonds dispersed in water surrounding the contact. The nanodiamonds were found to have a profound effect on the tribological performance at both nanometer and macroscopic scales. The tribological effects were highly sensitive to the sign of the nanodiamond electrical charge: negatively (positively) charged particles exhibited weaker (stronger) adhesion. Positively charged particles consistently increased friction at the solid-liquid interface, while negatively charged particles of comparable size were observed to decrease interfacial friction. For the macroscopic contacts with the gold electrodes, negatively charged nanodiamonds appeared to be displaced from the contact, while the positively charged ones were not. Overall, the negatively charged nanodiamonds were more stable in an aqueous dispersion over extended time periods while the positively charged nanodiamonds coagulated into larger particles and formed precipitates more quickly.

1. Introduction

Effective control of friction and wear addresses many urgent societal needs in such essential areas as energy efficiency, manufacturing, pharmaceuticals and the environment.^{1, 2} The total frictional losses in a typical diesel engine, for example, exceed 10% of the total energy of combustion.^{2, 3} Achieving even a modest 1% reduction in such losses would save between 10⁸ and 10⁹ gallons of diesel fuel annually in the U.S. alone – a significant saving from both economic and environmental viewpoints. Today's lubrication technologies were developed in an era that focused on wear elimination over friction energy losses with less attention paid to the environmental consequences. The most common lubrication additives in use today are based on sulphur-, phosphorous- and/or chlorine-containing compounds, which, together with the metal oxide powder generated during normal engine operation, render the waste oil a major environmental hazard.^{4, 5} These lubricant additives appear as one of the limiting factors for developing the next generation of structural materials for high efficiency

operating conditions. For example, tricresyl phosphate, which is an extremely efficient lubricant additive when used with iron-containing materials, is ineffective on stronger crack resistant chrome-based alloys.⁶⁻⁸ Unfortunately, it is also a known neurotoxin.⁹

Currently, different types of nanoparticulates are being actively pursued as alternatives to the traditional oil-based lubricant additives. Specifically, nanoparticulates composed of metals (*e.g.*, Zn, Al, Cu Ti, Fe) and their oxides,¹⁰⁻¹⁶ fluorinated compounds, graphitic nanoparticulates, and nanodiamonds¹⁷⁻¹⁹ have all shown to yield significant reductions in both friction (typically 10-20%) and wear when used as lubrication additives. Studies of the nanoparticulate additives have also been extended to nonpetroleum-based fluids, including water (*e.g.* fullerenols,²⁰ ZnO and Al₂O₃ nano-particulates^{11, 13, 21}) and ionic liquids (*e.g.* functionalized multi-walled carbon nanotubes²²). All of the abovementioned studies reported both a reduction in friction and an improved wear resistance.

One emerging class of effective anti-friction and wear-preventing nanoparticulates is comprised of nanodiamonds

obtained mechanically (*i.e.*, by crushing diamond crystals²³) or through detonation of an oxygen-deficient mixture of explosives.²⁴ Crushed nanodiamonds are typically 100-500 nm in diameter and have potential as solid lubricants in vacuum²³ whereas the detonation nanodiamonds (DNDs) are much smaller, typically 4-7 nm in diameter,²⁴ with a narrow size distribution. DNDs have shown to be effective as anti-friction and anti-wear additives to oil-based lubricants.^{17, 25-28} Recently, Osawa described eight- to tenfold reduction in the friction coefficients upon addition of 4 nm NDs to several polar liquids including water, ethylene glycol, and DMSO.²⁹ Given that the conventional additives to oil are insoluble or ineffective in aqueous and ionic liquid solvents, development of NDs as additives may ultimately allow for replacing the centuries-old oil-based lubricating technologies altogether after the essential technical criteria are met.²⁹

While the empirical search for the best combination of nanoparticles, lubricating fluids, and applicable surfaces continues, the fundamental understanding of the atomic scale mechanisms responsible for the macroscopic tribological performance is currently lacking in the literature. While experiments in vacuum with larger (>100 nm in diameter) NDs suggest that these hard spherical particles could play the role of rolling spacers between the contacting surfaces,²³ atomic scale surface phenomena³⁰ are expected to play a larger role for much smaller (*ca.* 5 nm diameter) DNDs, especially when used as additives to liquid lubricants. Suggested mechanisms include changes in the lubricant viscosity and thermal transport properties, formation of protective surface films, and surface smoothing through polishing and/or filling of the spaces between the contacting asperities. In addition to the “boundary lubrication” regime, the benefits of such nanolubricants have recently been demonstrated in elastohydrodynamic lubrication, where a reduced surface roughness in the rolling contact was achieved through polishing by the nanoparticles.³¹ Uptake of the nanoparticles on surfaces could also alter the slip conditions at the fluid-solid interface, thus, changing the system’s friction and wear attributes.³²⁻³⁵ Here, we examine the impact of the sign of the ND’s surface charge on the tribological properties in aqueous solutions, as virtually all the dispersed nanoparticles require surface charge to prevent coagulation and the eventual precipitation from a solution. At the macroscopic scale, both positive and negatively charged NDs are observed to reduce the friction coefficients, with surface polishing suggested as a possible mechanism^{28, 36} despite the fact that surface smoothening in general does not necessarily result in lower friction coefficients.³² Further investigations are therefore necessary to establish the underlying physical mechanisms.

To be effective as lubricant additives, nanoparticles must also exhibit long-term colloidal stability. Stability of such dispersions is known to be determined by the surface charge density that is typically characterized by the electrokinetic potential, or “zeta-potential”. It is the electrostatic repulsive force that prevents the dispersed nanoparticles from coagulation and consequent precipitation. Typically, a zeta potential of 25-30 mV (positive or negative) is sufficient to electrically stabilize a colloid.³⁷ DNDs can be produced with both positive and negative zeta potentials, thus, allowing for investigating the effects of the sign of the surface charge on tribological performance. Moreover, DND surfaces can be functionalized with a number of chemical groups to vary the zeta potential without compromising the diamond core properties.^{18, 29, 38-43} Functionalization so as to produce DNDs

with like-charged surfaces does not, however, guarantee that the DNDs will exhibit a mutual repulsion. There are numerous literature reports of an attraction between like-charged colloids in solutions and/or other environments where the charge rearrangements are possible when the particles approach each other.⁴⁴⁻⁴⁷

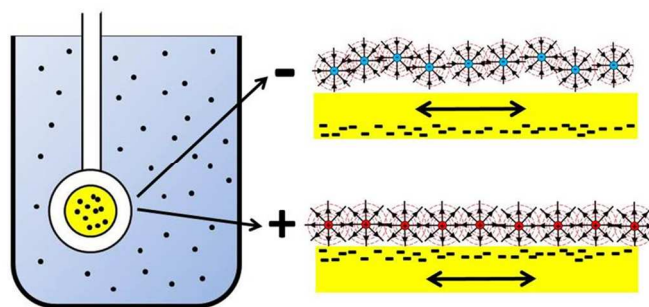


Fig. 1. A schematic illustration of the experimental QCM setup. (Left) A QCM holder (white) with a quartz crystal covered by a gold electrode (yellow) is immersed in an aqueous suspension of nanodiamonds (NDs). (Right) A cartoon of positively charged NDs adsorbed on a laterally oscillating QCM electrode with (bottom) interacting more strongly with the QCM electrode than the negatively charged ones (top).

Here we report on a Quartz Crystal Microbalance (QCM) study of surface uptake and the nanotribological properties of DNDs *ca.* 5-15 nm in diameter dispersed in water. QCM is an established tool for probing the tribological performance of material-liquid-nanoparticulate systems.^{32, 33, 35, 48, 49} It consists of a quartz single crystal that is electrically driven at its resonance frequency f_0 in a transverse shear motion (Fig. 1). Changes in the resonant frequency, δf , and the inverse quality factor, $\delta(Q^{-1})$, of the crystal are reflective of the material uptake and the mechanical dissipation properties (*e.g.*, flexibility, sliding friction, density) of materials deposited onto its surface electrodes and/or drag forces and slip lengths of the fluids by which it may be surrounded.

QCM measurements were performed with a crystal whose gold surface electrodes were immersed in aqueous suspensions of positively and negatively charged DNDs. As illustrated schematically in Figure 1, it is anticipated that mobile conduction electrons within the gold electrode may react differently to the uptake of the negatively and the positively charged DNDs. Specifically, an electrostatic attraction force between the positively charged DNDs and the negatively charged electrons is expected to result in relatively strong adhesion compared to a neutral nanodiamond. The negatively charged DNDs are expected to be relatively poorly bound to the surface and possibly reduce the friction through a reduction of drag forces with the surrounding liquid. Measurements were also performed with stainless steel ball bearings loaded onto the upper gold QCM electrode in the presence of a water layer containing either positively or negatively charged DNDs (Fig. 2). Our experimental data demonstrate profound changes in the tribological performance at both nano- and macroscopic scales in the presence of DNDs, and also highlight significance of the electrostatic phenomena as the tribological parameters were found to be strongly affected by the sign of the DNDs’ zeta potential.

2. Materials and Methods

2.1 Materials

All chemicals were purchased from Sigma-Aldrich (St. Louis, MO) or Acros Organics (Morris Plains, NJ).

Ball bearings, 316 stainless steel and 5/32" in diameter, model 316-5/2, were purchased from Bearing Ball Store (Orlando, FL).

DNDs were provided by the International Technology Center (Raleigh, NC). The samples were prepared by a detonation of an oxygen-deficient explosive mixture of trinitrotoluene with hexogen (40:60 wt%) in a closed steel chamber using ice as a cooling media.¹⁸ The product, detonation soot, was a mixture of up to 75% diamond particulates with other carbon allotropes, as well as metallic impurities. DNDs were purified by oxidation of the soot in an ozone-enriched air at 150-200 °C over 72 h.³⁸ The residual content of incombustible impurities in DNDs was estimated as ≈ 0.8 wt%. After the ozone purification, the resulting DND powder was light-grey in color. DNDs (10 wt%) were suspended in deionized (DI) water by sonication. Consequently, the suspensions were processed in a Retsch (Haan, Germany) planetary mill for 4 hrs using 100 μm zirconia beads. After the milling the product was treated in HF to remove contaminations from zirconia, washed with DI water, and re-suspended in DI water at 1 wt/v% by sonication. Centrifugation at 25,000 \times g for 2 hrs was used to extract DND particles with 5 \pm 2 nm in diameter as measured by dynamic light scattering (DLS) and zeta potential $\zeta \approx -45$ mV at neutral pH (sample (-S1), Table 1). An additional centrifugal fractionation was employed to separate DNS fractions with 10 \pm 2 and 15 \pm 2 nm diameters (samples (-S2) and (-S3), respectively, Table 1).

DNDs with a positive zeta potential ($\zeta \approx +45$ mV) were produced by a reduction reaction.³⁸ A suspension of the 5 nm DND with $\zeta \approx -45$ mV was initially air-dried. The dry powder (5 g) was added to a round-bottom flask and further dried using a Schlenk line and at least three nitrogen purge-and-refill cycles. Consequently, 20 ml of degassed anhydrous tetrahydrofuran (THF) and 50 mL of 2.0 M solution of LiAlH₄ in THF was added by a cannula. The sample was stirred under a nitrogen atmosphere at room temperature overnight. The reaction was quenched by a drop-wise addition of 1 M HCl, which solubilized the lithium and aluminum, and then pH of the solution was adjusted back to neutral. The product was collected by centrifugation and rinsed several times with water followed by a re-suspension in DI water by sonication and fractionation by centrifugation at 25,000 \times g for 2 hrs to extract 5 \pm 2 nm primary particles. While the 5 nm fully deagglomerated particles were used for the reduction reaction, during the functionalization some of the particles formed larger agglomerates requiring an additional fractionation to separate the 5 \pm 2 nm primary particles (sample (+S1), Table 1). All DNDs were stored as 5 w/v% colloids in DI.

Immediately before the QCM measurements, DND suspensions were sonicated for 20 min using an Aquasonic Model 75D (VWR International, Radnor, PA) bath sonicator at 23 °C. For Dynamic Light Scattering (DLS) measurements the suspensions were diluted twentyfold to reduce light scattering and drawn into a polystyrol/polystyrene cuvette (10 \times 10 \times 45 mm³). The size distributions and ζ -potential were measured at 25 °C using Zetasizer (Nano-ZS series, Malvern Co, U.K).

2.2 QCM electrode preparation

Polished AT-cut QCM crystals (1" diameter) with gold electrodes intended for liquid operation at 5 MHz overtone

frequency were purchased from Inficon (East Syracuse, NY). The data reported here were found to be independent of whether the electrodes were prepared with Au/Cr or Au/Ti layers. Prior to each run, the crystals were thoroughly washed with running tap water and then rinsed with DI water. Consequently, the crystals were submersed in 0.05 M NaOH solution for 30 minutes, air-dried, treated with UV ozone in PDS Series Digital UV Ozone system model PSD-UV4, Novascan Technologies, Inc. (Ames, IA) for 30 min, immersed in 190 proof ethanol for 30 min, treated again with UV ozone for 30 min, and then stored under dry nitrogen gas. This procedure is a slight modification of the standard cleaning protocol described elsewhere.^{50, 51}

2.3 QCM measurements

QCM data were collected using a QCM100 (Stanford Research Systems, Sunnyvale, CA, USA) system. The system includes a controller, oscillator electronics and a specialized Teflon holder that exposes one side of the crystal to the liquid while providing both mechanical support and electrical connections to the gold electrodes. A LabView (National Instruments, Austin, TX) PC-based data acquisition system was used to record both the crystal resonant frequency and the conductance voltage from the controller output. The conductance voltage, V_c , is related to the mechanical resistance, R_m , as $R_m = 10^{(4-V_c/5)} - 75$.⁵²

QCM measurements were carried out at room temperature in a glass beaker containing 150 ml of DI water. Temperature was further stabilized by placing the beaker into a StyrofoamTM container. After fully immersing the QCM holder into water and an initial stabilization of the QCM frequency, 1 weight% DND aqueous suspension was added portionwise (5 portions of 1.05 ml each at approximately 30 min intervals) via a pipette. Each portion contained 1.05 mg of DNDs. The color of the aqueous suspension became uniform in *ca.* 30 s after the injection indicating an effective mixing.



Fig. 2. Photograph of the QCM holder held horizontally with sixteen ball bearings loaded onto its surface electrode.

For the experiments with stainless steel ball bearings, the QCM crystals with gold electrodes were freshly cleaned by the procedure described in the section 2.2, placed in the Teflon holders in air, and then covered with 1.5 ml of either pure DI water, or an aqueous suspension containing positively or negatively charged DNDs. Sixteen ball bearings were placed atop the electrode in a pattern displayed in Fig. and the QCM response was recorded. The order in which water and ball bearings were added atop the electrode did not impact the QCM final response.

2.4 QCM data analysis

A QCM consists of a single crystal of quartz that is driven at its resonance frequency f_0 in a transverse shear motion by a voltage applied to the surface gold electrodes (*cf.* Fig. 1). As originally reported by Sauerbrey,⁵³ an additional rigidly

adhering film deposited onto one side of a QCM will decrease its resonant frequency by:

$$\delta f_{film} = -\left(\frac{m_f}{A}\right) \left(\frac{2f_0^2}{\sqrt{\rho_q \mu_q}}\right) = -2.264 \times 10^{-6} (\rho_2 f_0^2), \quad (1)$$

where $\rho_2 = (m_f/A)$ is the mass per unit area of the film in g/cm^2 , $\rho_q = 2.648 \text{ g/cm}^3$ is the density and $\mu_q = 2.947 \times 10^{11} \text{ g/cm}^2\text{s}^2$ is the shear modulus of quartz. Then one layer of 5 nm diameter spherical diamond nanoparticles packed in the closest hexagonal arrangement (assuming diamond bulk density of 3.5 g/cm^3 , mass per particle: $2.29 \times 10^{-19} \text{ g}$; area on the crystal surface per particle: 21.65 nm^2 , yielding $\rho_2 = 1.058 \times 10^{-6} \text{ g/cm}^2$) added atop of a 5 MHz QCM would result in a $\delta f_{film} = 59.8 \text{ Hz}$ decrease in the resonant frequency (cf. Eq.(1)).

If the adsorbed film slips on the QCM surface in a response to the oscillatory motion, the magnitude of the frequency shift δf_{film} will be lower than that given by the Eq.(1) for the rigidly attached film. There will also be a decrease in the QCM's quality factor, Q , since the friction associated with the film's sliding results in additional energy dissipation. For a film characterized by a frictional force per unit area $F/A = \eta v$, where v is the sliding speed, a characteristic "slip time", $\tau = \rho_2/\eta$ parameterizes the strength of the friction coefficient η and can be inferred from the relation $\delta(Q^{-1}) = 4\pi\tau(\delta f)$ if the shifts in both frequency and the dissipation associated with the presence of the film are monitored.⁵³

For a QCM immersed in a fluid with bulk density ρ_3 and viscosity η_3 , one would also observe δf and $\delta(Q^{-1})$ shifts from additional viscous drag forces and an increased inertia of the oscillator that under no-slip boundary conditions are given by:⁵⁴

$$\delta(Q^{-1}) = 2\alpha, \quad \delta f = -f_0\alpha, \quad \text{where } \alpha = \sqrt{\frac{\rho_3\eta_3 f_0}{\pi\rho_q\mu_q}}. \quad (2)$$

Therefore an immersion of one side of $f_0=5 \text{ MHz}$ QCM in water at room temperature ($\rho_3 = 1 \text{ g/cm}^3$, $\eta_3 = 0.01 \text{ poise}$) results in $\delta f = -714 \text{ Hz}$ drop in the resonant frequency and an increase of $\delta(Q^{-1}) = 2.85 \times 10^{-4}$ in the dissipation. For a QCM with quality factor $Q = 50,000$ in air this corresponds to a drop to $Q = 3,280$ after an immersion in water.

Although the viscous drag forces on the QCM electrode are mechanical in nature, a decrease in Q is manifested as an increase in the series resonant resistance R_m of the QCM resonator that can be measured electrically. For a QCM electrode exposed to a fluid from one side under non-slip conditions:⁵⁴

$$\delta R_m = \frac{1}{8K^2 C_0} \sqrt{\frac{\pi\rho_3\eta_3}{f_0\rho_q\mu_q}}, \quad (3)$$

where $K^2 = 7.74 \times 10^{-3}$ is the electromechanical coupling factor for the AT cut quartz and C_0 is the static capacitance of the QCM electrodes, including the parasitic capacitance associated with the connections to the oscillator circuit. A comparison of Eqs. (2) and (3) reveals that δR_m is directly proportional of $\delta(Q^{-1})$. This is expected since both parameters are reflective of the oscillator dissipative behaviour. For the QCM system employed here, the theoretical value for δR_m increase associated with the immersion of $f_0=5 \text{ MHz}$ QCM in water is approximately 300Ω .

A rigidly adhering monolayer of nanoparticles on a planar surface is expected to lower f_0 by an amount given by Eq.(1) with no additional shift in Q if the no-slip boundary condition is satisfied. If, however, the QCM surface is not perfectly planar, or the surface roughness and/or slip conditions at the boundary change upon the nanoparticles' uptake (surface polishing or filling by nanoparticles resulting in a smoother topology,

heterogeneous adhesion of the nanoparticles yielding a rougher surface, nanoparticles sliding at the interface, etc.), then the observed δf and $\delta(Q^{-1})$ shifts would reflect details of the underlying physical mechanisms.

2.5 Dynamic Light Scattering (DLS) measurements.

The sonicated DND were prepared by sonication using an Aquasonic Model 75D (VWR International, Radnor, PA) bath sonicator at $23 \text{ }^\circ\text{C}$ for 1.5 hr followed by 10 min centrifugation at 18078 g (Microfuge 18, Beckman.). For DLS measurements, 20 μL of sample (sonicated or non-sonicated) was diluted to 0.1% (W/V) and transferred to a disposable polystyrol/polystyrene cuvette and the sample size distribution was measured by DLS. The zeta potentials were measured for the same samples by placing them into a Zeta cell (Disposable folded capillary cell) and using Zeta potential measurement mode. All DLS measurements were performed at $25 \text{ }^\circ\text{C}$ using Nano-ZS series, Malvern co, U.K.

3. Results and discussion

3.1 Nanodiamond size and zeta potentials

Figure 3 shows size distributions of negatively and positively charged DNDs reconstructed from DLS experiments with twenty-fold diluted aqueous suspensions (final DND concentration of 0.25% w/v%) at $25 \text{ }^\circ\text{C}$. The negatively charged samples (-S1, -S2 and -S3) were stored as suspensions for ca. 2 years (solid lines) and re-sonicated just before the measurements (dashed lines). The positively charged DND sample (+S1) was not stable for the extended time periods displayed by the negatively charged suspensions: The solid line and dashed lines correspond to samples stored for several months. Analysis of DLS data for these aqueous suspensions of DNDs is summarized in Table 1 and the average zeta potential is plotted vs. average diameter in Fig.4.

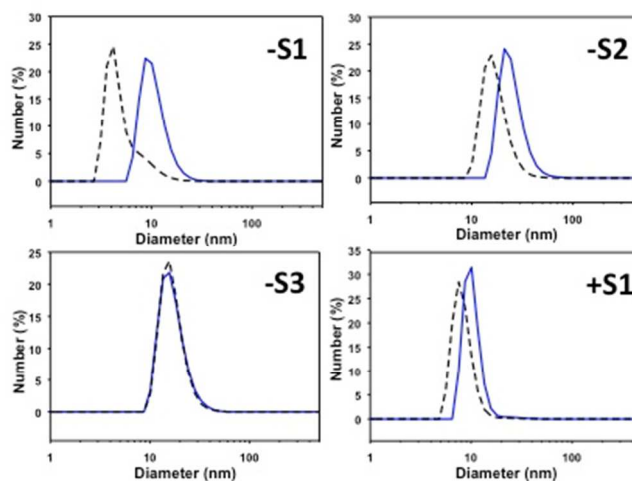


Fig. 3 Size distributions of positively and negatively charge DND's . Samples -S1, -S2 and -S3 as prepared were suspensions of negatively charged 5nm, 10nm and 15 nm samples. They were stored as suspensions for ca. 2 years (solid lines) and re-sonicated just before the measurements (dashed lines). Sample +S1 as prepared was a suspension of positively charged 5nm particles and was stored for several months (solid line) and re-sonicated just before the measurements (dashed line).

The smallest negatively charged DNDs (-S1) yielded remarkable resilience to the long term storage: while average

diameter of 5 ± 2 nm as-prepared particles increased to $d = 10.7 \pm 3.3$ nm after *ca.* 2 years in storage, the initial diameter was fully recovered after sonication (5.3 ± 2.5 nm, Table 1). After the sonication, the zeta-potential $\zeta = -41.8 \pm 2.8$ mV also recovered to $\zeta = -45$ mV specified for as-prepared particles. An interesting feature of the DND suspensions is that the particle size distributions after *ca.* 2 in storage either before or after the secondary sonication did not trend with the original as-prepared DNDs with the exception of sample (-S1). We therefore denote the samples according to their original sizes (Table 1).

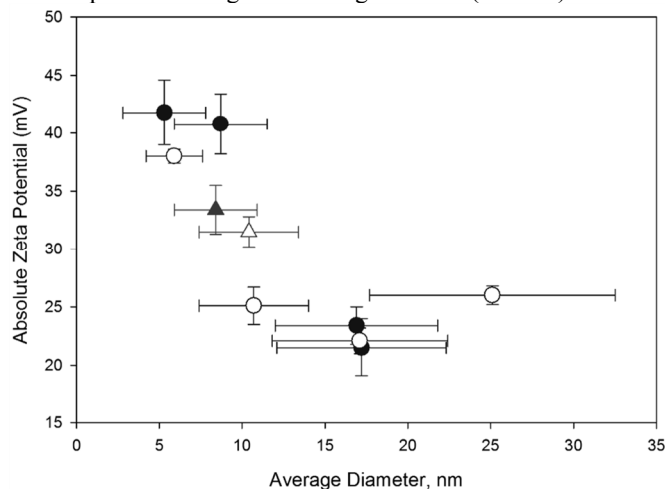


Fig. 4 Absolute values of the average zeta potential vs. average DND diameters for suspensions after *ca.* 2 yrs in storage. Triangles and circles represent the positively and negatively charged DNDs respectively. Open and filled symbols correspond to the DNDs before and after the secondary sonication respectively

For DND suspensions stored for *ca.* 2 years the secondary sonication decreases the average particle diameters for all but the (-S3) sample. However, the zeta potential did not change significantly except for the smallest 5 nm DNDs (-S1) which exhibit the highest magnitude of the zeta potential among all the samples studied. The general trend here is the smaller the DND, the higher the absolute value of the zeta potential. Fig. 4 shows the absolute value of the average zeta potential vs. average DND diameters for both negatively and positively charged particles. The zeta potential increases with decreasing particle diameter. This might be attributed to a higher charge density at the surface in smaller NDs that is essential for long-term stability of nanoparticle dispersions.³⁷

Table 1. Properties of DND nanoparticles from the analysis of DLS data.

Sample	DND preparation	Diameter (nm)	Zeta(ζ) potential, mV
(-S1)	As prepared	5 ± 2	-45 ± 2
	Stored <i>ca.</i> 2 yrs.	10.7 ± 3.3	-25.1 ± 1.6
	Sonicated after <i>ca.</i> 2 yrs.	5.3 ± 2.5	-41.8 ± 2.8
(-S2)	As prepared	10 ± 2	-35 ± 2
	Stored <i>ca.</i> 2 yrs.	25.1 ± 7.4	-26.0 ± 0.8
	Sonicated after <i>ca.</i> 2 yrs.	17.2 ± 5.1	-21.5 ± 2.5
(-S3)	As prepared	15 ± 2	-40 ± 2
	Stored <i>ca.</i> 2 yrs.	17.1 ± 5.3	-22.1 ± 1.1
	Sonicated after <i>ca.</i> 2 yrs.	16.9 ± 4.9	-23.4 ± 1.6
(+S1)	As prepared	5 ± 2.0	$+35 \pm 2$
	Freshly sonicated	8.4 ± 2.5	$+33.4 \pm 2.1$

3.2 Tribological properties of nanodiamonds interacting with gold surfaces

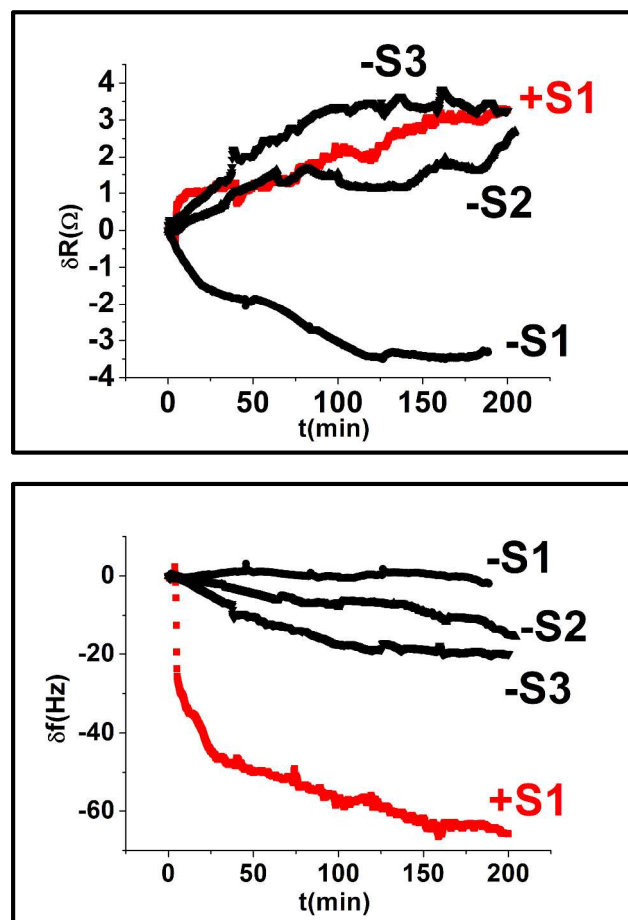


Fig. 5. Characteristic mechanical resistance, R_m (top) and frequency shift, δf (bottom), vs. time, t , of a 5 MHz QCM with one gold electrode surface submerged in water and exposed to DNDs whose original diameters were 5 nm (-S1 and +S1), 10 nm (-S2) and 15 nm (-S3). Portion-wise additions of 1 ml of 1 weight% aqueous suspension of positively (red) and negatively (black) charged nanodiamonds were added at $t = 0$ and approximately every 30 minutes thereafter.

All QCM experiments with positively and negatively charged DNDs were conducted at least in triplicate using different electrodes, and only minor deviations were observed between the individual runs with the same types of DNDs. The QCM response was dominated by the introduction of the first portion of the nanodiamonds, indicating that it was dominated by the surface and the interfacial effects near the electrode and not the concentration of nanodiamonds in the surrounding liquid. The QCM response was strikingly different for DNDs of opposite electrical charges. Figure 5 shows characteristic frequency shift and mechanical resistance data with time $t=0$ set to the moment of the first addition of DNDs and subsequent additions approximately every 30 minutes thereafter. Notably, observed changes in the frequency and the mechanical resistance cannot be attributed to an increase in viscosity of the liquid surrounding the QCM (*cf.* Eqs. (2,3)), as doubling and quadrupling the DND content failed to result in an additional

significant response (Fig. 5). The data show a clear trend in both resistance and frequency shift, with more uptake and more resistance for the large sized particles. In no case however does the uptake become comparable to that of the response of the positively charged sample denoted by +S1, whose original size as prepared was 5nm, but was more likely to be closer to 10nm in size as the measurements were recorded given the poor size stability of the positively charged samples.

Fig. 5 (lower) demonstrates that after *ca.* 3 hrs the frequency response of QCM stabilizes at $\delta f \approx -60$ Hz for the positively charged sample, corresponding to approximately one monolayer of the positively charged $d \approx 12.3$ nm DND particles attached to the electrode while the frequency shift associated with the addition of the negatively charged DNDs was negligible and even, in some cases, positive. The positive sign of δf is indicative of particles being present near the surface (since there was an impact on R_m), but exhibiting a high degree of slip and, thus, no significant increase in the inertia of the oscillator due to the negligible mass loading.

The mechanical resistance R_m of the QCM-liquid interface meanwhile increased by approximately 3Ω for the positively charged DNDs and decreased by approximately the same 3Ω when negatively charged 5nm DNDs were injected. The experiments clearly revealed a dramatic influence of the DND surface charge arising from various chemical groups on the nanoparticles' surface³⁸ on the system's nanotribological response. A possible explanation of the observed changes in f and R_m is that there is a strong electrostatic attraction between positively charged DNDs and the gold electrode surface while the negatively charged particles are physically adsorbed to the surface but also undergo significant slip in response to the lateral oscillations of the QCM. The effect clearly weakens for negatively charged nanoparticles whose zeta potentials are significantly smaller (Table 1). This scenario is depicted schematically in Fig 1, where mobile conduction electrons within the gold electrode are attracted or repelled from the surface, depending on the charge of the adsorbed nanodiamonds. This scenario would also explain the higher frictional drag forces observed for the surrounding liquid, as the surface topology could be more corrugated with bound, and more rigidly associated DNDs at the solid-liquid contact than the bare gold electrodes.

3.3 Macroscopic contact measurements

QCM response was also monitored for stainless steel ball bearings placed on top of the upper gold electrode (Fig. 2). Addition of ball bearings in the presence of a water layer resulted in an increase in both the frequency and the resistance for pure water or when an aqueous suspension of the negatively charged DNDs was used. However, the frequency commonly decreased for positively charged nanodiamonds.

In some experiments the QCM response reached the values as high as $\delta f = \pm 200$ Hz. Typical values for the QCM response upon immersion of one of the gold electrodes in liquid followed by loading of sixteen close-packed ball bearings are summarized in the Table 2. This is consistent with the mobile negatively charged nanodiamonds being displaced from the tribological contact, since the response for water with negatively charged ND is quite similar to pure water alone. In particular, the frequency increases when the ball bearings are placed on the electrode, indicating that contact stiffness effects are dominant over mass loading effects.^{55,56} The reverse is true however for the case of positive nanodiamonds, where mass

loading effects as reflected by negative frequency shifts are dominant. This is consistent with the positive nanodiamonds remaining within the tribological contact (Table 2).

Table 2. Characteristic QCM response to placement of sixteen stainless steel ball bearings atop gold electrodes immersed in pure water, water with positive ND additives, and water with negative ND additives.

	f (Hz)	δR_m (ohms)
Pure water	+102 +/- 22	8 +/- 20
Water with -ND	+76 +/- 28	13 +/- 22
Water with +ND	-9 +/- 2	6 +/- 20

4. Conclusions

Uptake and nanotribological properties of aqueous dispersions of positively and negatively charged DNDs and effects of these suspensions on tribological contacts between the macroscopic stainless steel ball bearings and gold electrodes were studied by means of QCM. It was observed that the nanoparticulates have a profound effect on both nanometer scale and macroscopic tribological performance and that the system response was highly sensitive to the sign of the nanodiamond electrical charge. While the magnitude of the QCM response somewhat varied from experiment to experiment, the positively charged nanodiamonds appear to be bound to the QCM electrode more strongly than the negatively charged ones. Adsorption of a monolayer of positively charged nanodiamonds on the electrode gold surface increases the frictional drag at the solid-liquid interface. In a striking contrast, all of the negatively charged DND's appear to be weakly bound to the surface and likely to exhibit a high degree of slip at the solid-liquid interface.

For the macroscopic contacts with the gold electrodes, the negatively charged nanodiamonds appeared to be entirely displaced from the contact, while the positively charged nanodiamonds were not.

Overall, the study shows the potential of QCM to study tribological properties of nanoparticle dispersions and nanodiamonds in particular.

Acknowledgements

Support from NSF DMR0805204 (JK), NSF DMR1310456 (JK) and NSF DMMI1229889 (DB, OS) are gratefully acknowledged. Characterization of nanoparticles and the overall manuscript preparation was supported by U.S. DOE Contract DE-FG02-02ER15354 to AIS. JK appreciates insightful discussions with W.A. Henderson.

Notes and references

^a North Carolina State University, Raleigh, NC 27695, USA, E-mail: jkrim@ncsu.edu; Tel: +1 919 513 2684

^b International Technology Center, 8100 Brownleigh Dr, Raleigh, NC 27617, USA.

1. H. P. Jost, *Tribology & Lubrication Technology*, 2005, **61**, 18-22.
2. K. Holmberg, P. Andersson and A. Erdemir, *Tribology International*, 2012, **47**, 221-234.

3. K. Holmberg, P. Andersson, N. O. Nylund, K. Makela and A. Erdemir, *Tribology International*, 2014, **78**, 94-114.
4. C. I. Betton, in *Chemistry and Technology of Lubricants*, eds. R. M. Mortier and S. T. Orszulik, Springer Netherlands, 1997, ch. 13, pp. 349-370.
5. *Chemistry and Technology of Lubricants, Third Edition*, Springer-Verlag Berlin, Berlin, 2010.
6. C. S. Saba and N. H. Forster, *Tribology Letters*, 2002, **12**, 135-146.
7. M. Abdelmaksoud, J. W. Bender and J. Krim, *Tribology Letters*, 2002, **13**, 179-186.
8. M. Abdelmaksoud, J. W. Bender and J. Krim, *Physical Review Letters*, 2004, **92**.
9. S. G. Somkuti, H. A. Tilson, H. R. Brown, G. A. Campbell, D. M. Lapadula and M. B. Abou-Donia, *Toxicological Sciences*, 1988, **10**, 199-205.
10. S. Q. Qiu, Z. R. Zhou, J. X. Dong and G. X. Chen, *Journal of Tribology-Transactions of the Asme*, 2001, **123**, 441-443.
11. J. X. Dong and Z. S. Hu, *Tribology International*, 1998, **31**, 219-223.
12. Z. S. Hu and J. X. Dong, *Wear*, 1998, **216**, 92-96.
13. Z. S. Hu, J. X. Dong and G. X. Chen, *Tribology International*, 1998, **31**, 355-360.
14. B. Li, X. Wang, W. Liu and Q. Xue, *Tribology Letters*, 2006, **22**, 79-84.
15. A. H. Battez, R. Gonzalez, J. L. Viesca, J. E. Fernandez, J. M. D. Fernandez, A. Machado, R. Chou and J. Riba, *Wear*, 2008, **265**, 422-428.
16. R. Chou, A. H. Battez, J. J. Cabello, J. L. Viesca, A. Osorio and A. Sagastume, *Tribology International*, 2010, **43**, 2327-2332.
17. O. Elomaa, J. Oksanen, T. J. Hakala, O. Shenderova and J. Koskinen, *Tribology International*, 2014, **71**, 62-68.
18. V. N. Mochalin, O. Shenderova, D. Ho and Y. Gogotsi, *Nat. Nanotechnol.*, 2012, **7**, 11-23.
19. O. Elomaa, T. J. Hakala, V. Myllymaki, J. Oksanen, H. Ronkainen, V. K. Singh and J. Koskinen, *Diamond and Related Materials*, 2013, **34**, 89-94.
20. Y. H. Liu, X. K. Wang, P. X. Liu, J. P. Zheng, C. Y. Shu, G. S. Pan and J. B. Luo, *Science China-Technological Sciences*, 2012, **55**, 2656-2661.
21. S. Radice and S. Mischler, *Wear*, 2006, **261**, 1032-1041.
22. B. G. Wang, X. B. Wang, W. J. Lou and J. C. Hao, *Journal of Physical Chemistry C*, 2010, **114**, 8749-8754.
23. A. V. Gubarevich, S. Usuba, Y. Kakudate, A. Tanaka and O. Odawara, *Jpn. J. Appl. Phys. Part 2 - Lett. Express Lett.*, 2004, **43**, L920-L923.
24. N. R. Greiner, D. S. Phillips, J. D. Johnson and F. Volk, *Nature*, 1988, **333**, 440-442.
25. V. Y. Dolmatov, *J. Superhard Mater.*, 2010, **32**, 14-20.
26. C. C. Chou and S. H. Lee, *Wear*, 2010, **269**, 757-762.
27. S. H. Jun, Y. R. Uhm and C. K. Rhee, *Journal of Korean Powder Metallurgy Instit*, 2011, **18**, 417-422.
28. O. Shenderova, A. Vargas, S. Turner, D. M. Ivanov and M. G. Ivanov, *Tribology Transactions*, 2014, **57**, 1051-1057.
29. E. Osawa, in *Handbook of Advanced Ceramics: Materials, Applications, Processing, and Properties, 2cd. ed.*, S. Somaya, ed, (Elsevier, 2013) pp89-102.
30. D. Berman, S. A. Deshmukh, S. K. R. S. Sankaranarayanan, A. Erdemir and A. V. Sumant, *Science*, 2015, **348**, 1118-1122.
31. M. Mosleh and K. A. Shirvani, *Wear*, 2013, **301**, 137-143.
32. J. Krim, *Advances in Physics*, 2012, **61**, 155-323.
33. K. Huang and I. Szlufarska, *Langmuir*, 2012, **28**, 17302-17312.
34. S. Granick, Y. X. Zhu and H. Lee, *Nature Materials*, 2003, **2**, 221-227.
35. K. Huang and I. Szlufarska, *Physical Review E*, 2014, **89**.
36. N. Nunn, Z. Mahbooba, M. G. Ivanov, D. M. Ivanov, D. W. Brenner and O. Shenderova, *Diamond and Related Materials*, 2015, **54**, 97-102.
37. M. Kaszuba, J. Corbett, F. M. Watson and A. Jones, *Philosophical Transactions of the Royal Society a-Mathematical Physical and Engineering Sciences*, 2010, **368**, 4439-4451.
38. O. Shenderova, A. Koscheev, N. Zaripov, I. Petrov, Y. Skryabin, P. Detkov, S. Turner and G. Van Tendeloo, *Journal of Physical Chemistry C*, 2011, **115**, 9827-9837.
39. A. M. Schrand, S. A. C. Hens and O. A. Shenderova, *Crit. Rev. Solid State Mat. Sci.*, 2009, **34**, 18-74.
40. F. Gareeva, N. Petrova, O. Shenderova and A. Zhukov, *Colloids and Surfaces a-Physicochemical and Engineering Aspects*, 2014, **440**, 202-207.
41. A. Kruger, F. Kataoka, M. Ozawa, T. Fujino, Y. Suzuki, A. E. Aleksenskii, A. Y. Vul and E. Osawa, *Carbon*, 2005, **43**, 1722-1730.
42. T. Tyler, V. V. Zhirnov, A. V. Kvit, D. Kang and J. J. Hren, *Applied Physics Letters*, 2003, **82**, 2904-2906.
43. L. C. L. Huang and H. C. Chang, *Langmuir*, 2004, **20**, 5879-5884.
44. M. Deserno, A. Arnold and C. Holm, *Macromolecules*, 2003, **36**, 249-259.
45. T. E. Angelini, H. Liang, W. Wriggers and G. C. L. Wong, *Proceedings of the National Academy of Sciences*, 2003, **100**, 8634-8637.
46. J. C. Butler, T. Angelini, J. X. Tang and G. C. L. Wong, *Physical Review Letters*, 2003, **91**.
47. J. Lekner, *Electrostatics of two charged conducting spheres*, 2012.
48. M. Rodahl, F. Hook, A. Krozer, P. Brzezinski and B. Kasemo, *Review of Scientific Instruments*, 1995, **66**, 3924-3930.
49. M. Rodahl and B. Kasemo, *Review of Scientific Instruments*, 1996, **67**, 3238-3241.
50. A. Ulman, *An introduction to ultrathin organic films : from Langmuir-Blodgett to self-assembly*, Academic Press, Boston, 1991.
51. J. B. Brzoska, I. B. Azouz and F. Rondelez, *Langmuir*, 1994, **10**, 4367-4373.
52. *Stanford Research Systems. QCM 100 Quartz Crystal Microbalance User Manual, Chapter 2*, p. 11.
53. G. Sauerbrey, *Zeitschrift Fur Physik*, 1959, **155**, 206-222.
54. K. K. Kanazawa and J. G. Gordon, *Anal. Chim. Acta*, 1985, **175**, 99-105.
55. B. Borovsky, J. Krim, S.A. Syed Asif and K.J. Wahl, *J. Appl. Phys.*, 2000, **90**, 6391-6396
56. A. Laschitsch and D. Johannsmann, *J. Appl. Phys.*, 1999, **85**, 3759-3765